Monthly Notices
of the
ROYAL ASTRONOMICAL SOCIETY

MNRAS **436,** 531–539 (2013)
Advance Access publication 2013 September 26

doi:10.1093/mnras/stt1590

Double-diffusive magnetic buoyancy instability in a quasi-two-dimensional Cartesian geometry

D. M. Skinner⋆ and L. J. Silvers⋆

Centre for Mathematical Science, City University London, Northampton Square, London, EC1V 0HB, UK

Accepted 2013 August 21. Received 2013 August 21; in original form 2012 January 19

ABSTRACT

Magnetic buoyancy, believed to occur in the solar tachocline, is both an important part of large-scale solar dynamo models and the picture of how sunspots are formed. Given that in the tachocline region the ratio of magnetic diffusivity to thermal diffusivity is small it is important, for both the dynamo and sunspot formation pictures, to understand magnetic buoyancy in this regime. Furthermore, the tachocline is a region of strong shear and such investigations must involve structures that become buoyant in the double-diffusive regime which are generated entirely from a shear flow. In a previous study, we have illustrated that shear-generated double-diffusive magnetic buoyancy instability is possible in the tachocline. However, this study was severely limited due to the computational requirements of running three-dimensional magnetohydrodynamic simulations over diffusive time-scales. A more comprehensive investigation is required to fully understand the double-diffusive magnetic buoyancy instability and its dependency on a number of key parameters; such an investigation requires the consideration of a reduced model. Here we consider a quasi-two-dimensional model where all gradients in the x direction are set to zero. We show how the instability is sensitive to changes in the thermal diffusivity and also show how different initial configurations of the forced shear flow affect the behaviour of the instability. Finally, we conclude that if the tachocline is thinner than currently stated then the double-diffusive magnetic buoyancy instability can more easily occur.

Key words: instabilities – MHD – Sun: interior – Sun: magnetic fields.

1 INTRODUCTION

The leading models of the large-scale solar dynamo posit that a toroidal magnetic field is generated from a poloidal field deep beneath the surface of the Sun in the tachocline (see e.g. Silvers 2008; Charbonneau 2010, and references therein). The toroidal structures then become buoyant and rise towards the surface. The strongest of these magnetic filaments reach the surface to give rise to sunspot pairs. The weaker buoyant structures can be twisted in the solar convection zone, which is an important part of one large-scale dynamo model, namely, the interface model (Parker 1993). Therefore, given that the process of magnetic buoyancy is an integral part of both the sunspot formulation picture and models of the large-scale solar dynamo, it is crucial that it is fully understood.

Magnetic buoyancy was first discussed by Parker (1955) and Jensen (1955) and since this time there has been considerable progress in understanding this process. Early research using linear stability analysis derived stability criteria for ideal magnetohydrodynamics and diffusive magnetohydrodynamics (see e.g. Parker 1966; Thomas & Nye 1975; Acheson 1979).

In the solar tachocline, while diffusivities are small they are non-negligible. Therefore, the most pertinent of these criteria to consider for structures in the tachocline is that derived by Acheson (1979):

$$\frac{-ga^2}{c^2}\frac{\mathrm{d}}{\mathrm{d}z}\ln B > \frac{\eta}{\kappa}N^2 \tag{1}$$

where B is the field strength, η is the magnetic diffusivity, κ is the thermal diffusivity, a is the Alfvén speed, c is the adiabatic sound speed and N is the Brunt–Väisälä frequency. In the tachocline, $\kappa \gg \eta$ and it is this regime that we need to explore fully; this paper will focus on the magnetic buoyancy instability when $\kappa \gg \eta$. Given that the magnetic structures in the tachocline are generated by a shear flow it is important to numerically examine structures that are generated in this way as opposed to simply examining those that are unstable at the start of the simulation.

⋆E-mail: david.skinner.1@city.ac.uk (DMS); Lara.Silvers.1@city.ac.uk (LJS)

Seeking to understand the formation of shear generated magnetic buoyant structures is a complex issue because of the dynamic nature of the problem, which involves a number of different time-scales i.e. the advective time-scale associated with the generation of a layer of magnetic field, the time-scale associated with the instability and the diffusive time-scales. In this particular problem a shear flow will drag out a layer of magnetic field that is initially perpendicular to the direction of the large-scale flow. This will create gradients in the magnetic field, which are necessary to achieve for buoyancy as can be seen from criterion 1. However, the layer of magnetic field acts back on the flow, which reduces the shear flow's effectiveness to generate gradients of magnetic field. Further, the background atmosphere will be altered and so the values of the components in criterion 1 for instability are constantly changing.

Research to date on the interaction between a shear flow and a magnetic field includes that of Tobias & Hughes (2004) who examined the stability of an atmosphere where there is a flow aligned with the magnetic field and concluded that the shear has a stabilizing effect on the magnetic buoyancy instability. However, in the tachocline the shear is actually responsible for the generation of an unstable layer of magnetic field aligned with the shear flow where, in an idealized picture, none exists; this is a very different proposition. There have been a number of papers to examine shear generated magnetic buoyancy instabilities when the magnetic field is not initially in the direction of the shear flow (Cline, Brummell & Cattaneo 2003; Vasil & Brummell 2008; Silvers et al. 2009). Silvers et al. (2009) considered if the double-diffusive magnetic buoyancy instability could occur in the tachocline and were the first to numerically show that such an instability is plausible. This work follows earlier calculations and discussions (see Hughes & Weiss 1995; Schmitt & Rosner 1983, and references there in) regarding a magnetic buoyancy instability that presents when the ratio of magnetic to thermal diffusivity becomes sufficiently small, i.e. a double-diffusive magnetic buoyancy instability.

While the work of Silvers et al. (2009) was pioneering in the area of numerical calculations of the double-diffusive instability, their investigation was inhibited by the computational costs associated with three-dimensional calculations using small diffusivities. As such, they were only able to conduct a very limited investigation into how the instability is affected by the parameters that appear in the formulation of the problem and, thus, a further investigation is warranted.

While the investigation of Silvers et al. (2009) was limited, it was sufficient to show that the initial stages of the instability are dominated by the rapid growth of two-dimensional modes. This finding is in agreement with works such as Newcomb (1961) that suggest that two-dimensional interchange modes will often present rather than three-dimensional bending modes. That said, modes that initially onset in a two-dimensional fashion can develop in a three-dimensional way though interactions with other motion, e.g. turbulence caused by descending convective plumes, and so are of interest when we are looking for long-term, three-dimensional buoyant structures and their evolution.

The work of Silvers et al. (2009) suggests that a useful avenue of investigation, to explore further how the various parameters affect the onset of the double-diffusive magnetic buoyancy instability, is through a reduced model, which will minimize the computational cost of exploring the parameter space. Such a model will be considered in this paper where we wish to obtain a greater understanding of the onset parameters for double-diffusive magnetic buoyancy instabilities, which will be used in later calculations to investigate the three-dimensional evolution of these structures. The reduced model that we use in this paper is such that gradients in the x-direction are neglected. This reduction permits a much fuller exploration of the parameter space and enables us to determine how certain parameters affect the onset of the instability and the growth rate.

2 NUMERICAL MODEL

We consider a model similar to those presented in the three-dimensional work of Silvers et al. (2009) and Vasil & Brummell (2008) but we form a reduced model by neglecting gradients in one direction. In this work the x and y coordinates are the latitudinal and longitudinal directions, and the z-axis points vertically down and parallel to the constant gravitational acceleration. All lengths are scaled relative to the depth of the domain, d. The temperature, T, is scaled relative to T_*, the temperature at the top of the domain. The density, ρ, is scaled relative to ρ_* the density at the top of the layer. The magnetic field, $\boldsymbol{B}$, is scaled relative to the initial vertical magnetic field strength, $B_{z,0}$. Time is scaled with the isothermal sound crossing time at the top of the layer, $\tau_* = d\rho_*^{1/2}/P_*^{1/2}$. The general governing equations are written in the form:

$$\frac{\partial \rho}{\partial t} + \nabla.(\rho \boldsymbol{v}) = 0, \tag{2}$$

$$\rho\left(\frac{\partial \boldsymbol{u}}{\partial t} + \boldsymbol{u}\,.\,\nabla \boldsymbol{u}\right) = -\nabla P + \alpha\,(\boldsymbol{B}\,.\,\nabla)\,\boldsymbol{B} - \alpha\nabla\left(\frac{B^2}{2}\right) + \sigma C_k\left(\nabla^2 \boldsymbol{u} + \frac{1}{3}\nabla\,(\nabla\,.\,\boldsymbol{u})\right) + \rho\theta\,(m+1)\,\hat{\boldsymbol{z}} + \boldsymbol{F} \tag{3}$$

$$\frac{\partial T}{\partial t} = -\boldsymbol{u}\,.\,\nabla T - (\gamma - 1)\,T\nabla\,.\,\boldsymbol{u} + \frac{C_k\gamma}{\rho}\nabla^2 T + \frac{C_k\,(\gamma-1)}{\rho}\left(\alpha\zeta J^2 + \frac{\sigma}{2}S^2\right) \tag{4}$$

$$\frac{\partial \boldsymbol{B}}{\partial t} = \nabla \times (\boldsymbol{u} \times \boldsymbol{B}) + \zeta C_k \nabla^2 \boldsymbol{B}, \tag{5}$$

$$\nabla\,.\,\boldsymbol{B} = 0 \tag{6}$$

where

$$S_{ij} = \frac{\partial u_i}{\partial x_j} + \frac{\partial u_j}{\partial x_i} - \frac{2}{3}\frac{\partial u_k}{\partial x_k}\delta_{ij} \tag{7}$$

is the stress tensor. $C_k = K\tau_*/\rho_* c_p d^2$ is the dimensionless thermal diffusivity, $\alpha = B_{z,0}^2/P_*\mu_0$ provides a measure of the field strength, $\zeta = \eta c_p \rho_*/K$ is the inverse Roberts number, $\sigma = \mu c_p \rho_*/K$ is the Prandtl number, θ is the thermal stratification and m is the polytropic index.

Equation (3) has been augmented to include an extra body force, $\boldsymbol{G} = -\sigma C_k \partial_z^2 U_0\,(z)\,\hat{\boldsymbol{x}}$ that, in the absence of magnetic effects or instabilities, balances viscous diffusion and maintains a specified $U_0(z)$, which is chosen to mimic the smooth radial shear transition believed to occur in the tachocline. The shear profile is given by

$$U_0\,(z) = M\tanh\left[\frac{1}{\Delta z}\left(z - \frac{1}{2}\right)\right]. \tag{8}$$

Fig. 1 shows the velocity shear profile plotted against depth z for the initial parameter configuration where $M = 0.05$ and $\Delta z = 0.1$.

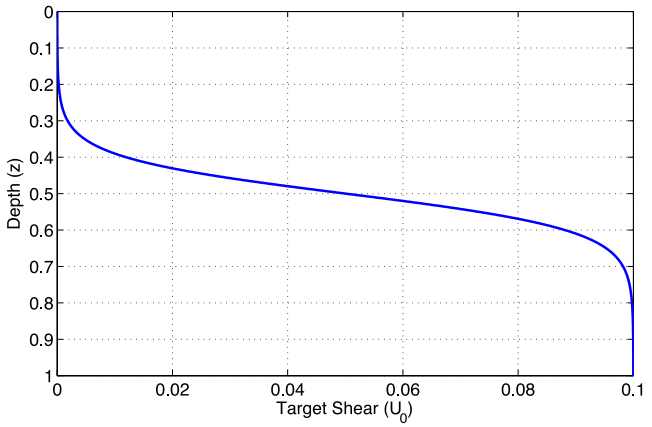

Figure 1. Shear profile, $U_0(z)$, versus depth, z, for the case used for the initial cases where $M = 0.05$ and $\Delta z = 0.1$.

The above set of equations is further simplified by removing all gradients of quantities in the x-direction, i.e. we set

$$\frac{\partial}{\partial x} f\,(x, y, z, t) = 0 \tag{9}$$

for all quantities.

Boundary conditions for the velocity, $\boldsymbol{v}$, and the magnetic field, $\boldsymbol{B}$, are $\partial_z u = \partial_z v = w = 0$ and $B_x = B_y = \partial_z B_z = 0$ at the top and bottom of the domain, $z = 0$, 1. The boundary conditions for temperature are $T(z = 1) = 1$ and $\partial T_z\,(z = 0) = \theta$. Periodic boundary conditions are taken in both the x and the y directions. These simulations are conducted using resolutions up to 256×480.

Initially we take a polytropic atmosphere with temperature $T_0 = 1 + \theta\hat{z}$ and density $\rho_0 = (1 + \theta\hat{z})^m$. We also initially set $B_z = 1$, $u_x = U_0(z)$, $u_y = u_z = B_x = B_y = 0$. The system is forced out of equilibrium state by a small initial random perturbation to the temperature field. The governing equations are solved using a mixed finite difference/pseudo-spectral scheme as discussed in, for example, Bushby & Houghton (2005).

In this investigation we will allow a number of parameters to vary but there are some parameters that will remain fixed for the entire paper. For all of the cases that we consider in our investigation we take $F = 1.25 \times 10^{-5}$, $\theta = 5$ and $m = 1.6$.

3 RESULTS

The double-diffusive magnetic buoyancy instability relies on the ratio between the magnetic and thermal diffusivities being small. Accordingly, the main focus of this paper is to see how the onset and growth rate of the instability, not its non-linear evolution, are affected by changing this ratio. Hence we will begin by examining the effect on the onset of the instability of varying the dimensionless thermal diffusivity, C_k. We note here that, for all results presented in this paper the Richardson number is such that the shear flow is stable, i.e. there is no secondary instability that can influence the results.

In this investigation we choose principally to adjust the ratio of magnetic to thermal diffusivities by varying the thermal diffusivity (via its dimensionless counterpart C_k). As we vary C_k we also adjust the Prandtl number, σ, and the inverse Roberts number, ζ, so as to maintain $\sigma C_k = 2.5 \times 10^{-6}$ and $\zeta C_k = 5.0 \times 10^{-6}$ thus leaving the form of the induction equation unchanged and changing the dynamics through the temperature equation. This method ensures that the magnetic Prandtl number is fixed, which aids

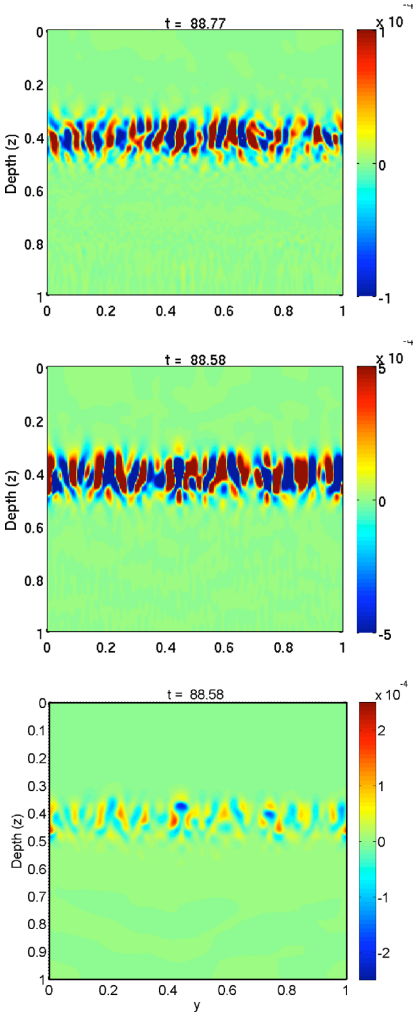

Figure 2. A comparison of the vertical component of velocity at comparable times for a slice of the three-dimensional case (top) and a quasi-two-dimensional run (middle). The bottom image shows density perturbation from the horizontal averaged value.

comparison with the work of Silvers et al. (2009). It is also possible to vary the inverse Roberts number, ζ, effectively varying the magnetic diffusivity without scalings and so changing the dynamics directly through the induction equation (5). This would give rise to a variable magnetic Prandtl number. For brevity we limit the full discussion here to considering the case where C_K is varied but we will make comment at the end about the effect of varying the magnetic diffusivity.

Before we commence our investigation, we begin by illustrating that this reduced model captures the essential dynamics of fully three-dimensional calculations, such as those shown in Silvers (2008). Fig. 2 shows a comparative slice from a fully three-dimensional and a quasi-two-dimensional calculation after the onset of the instability for the same set of parameters (case A1 in Table 1). Both simulations were started from the equilibrium solution with the same, small amplitude perturbation, to the temperature value at each point.[1] The resolution for the three-dimensional case is

[1] Note the image shown in Silvers et al. (2009) was started and evolved at early times in a slightly different way and found a slightly different lengthscale for the instability.

Table 1. Critical values for instability for different values of Δz.

Δz	Critical value
5.0×10^{-2}	6.355×10^{-4}
6.67×10^{-2}	7.692×10^{-4}
1.0×10^{-1}	1.137×10^{-3}

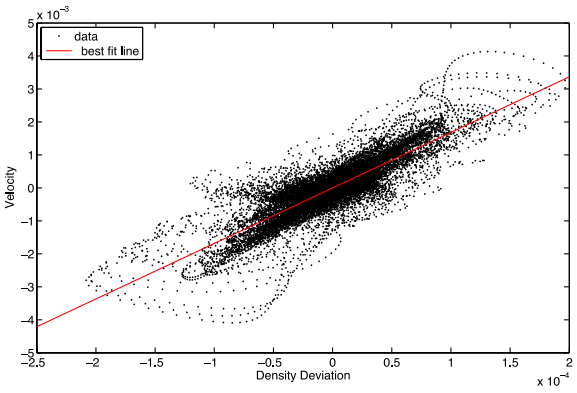

Figure 3. A scatter plot formed from the data at each point for the vertical velocity and the density perturbation from the horizontal average.

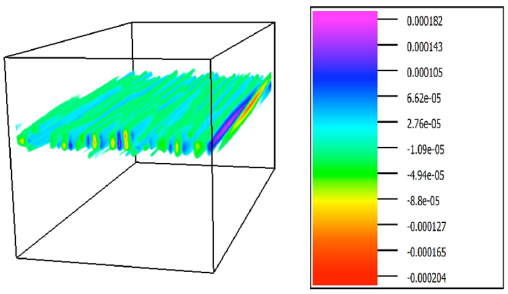

Figure 4. A volume rendering of vertical velocity taken at the same instance as the slices shown in Fig. 2 for case A1 and shows the initial two-dimensional nature of the instability.

256×256×480 and the resolution for the quasi-two-dimensional case is 256×480. Fig. 2 shows that, although the two slices are not exactly identical for the different calculations, the instability onsets with the same lengthscale. Fig. 2 also shows the density deviation from the layer average value and shows that the rising structures are less dense, as you would expect with structures arising from a buoyancy instability. The formal correlation between vertical velocity and the density deviation from the layer average at the time of the images shown in Fig. 2 is given in Fig. 3. This scatter plot shows a good agreement between the two quantities. Further, Fig. 4 shows that, as discussed in Silvers (2008), the instability onsets in a two-dimensional form. Thus, our reduced model captures the essential features of the fully three-dimensional calculation.

We commence our discussion of our findings by varying the ratio of magnetic to thermal diffusivities via varying C_k. The Richardson numbers, together with all of the exact parameter combinations for these cases, are given in a table in the Appendix. The background magnetic field is initially uniform in the z-direction. During the initial stages of the simulation there is a build up of the x component of the magnetic field as the z component is stretched out by the shear flow. During this period, the y component of the magnetic field undergoes small fluctuations due to the initial perturbation of

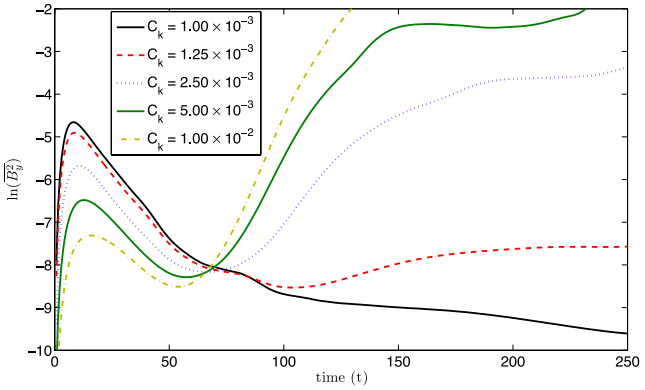

Figure 5. $\ln B_y^2$ versus time for different values of the dimensionless thermal diffusivity, C_k. The data points correspond to cases A1–A10 shown in Table A1.

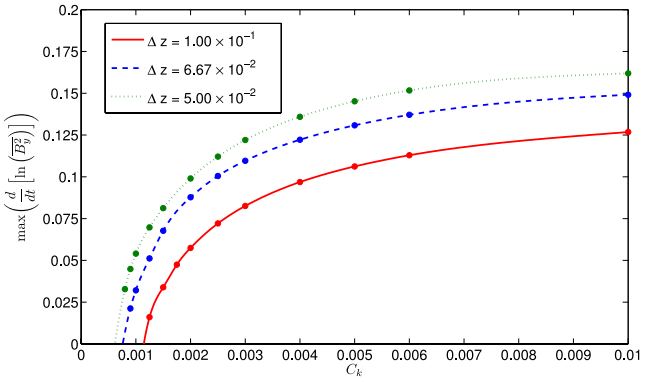

Figure 6. The maximum value of $\mathrm{d}(\ln B_y^2)/\mathrm{d}t$ versus the dimensionless thermal diffusivity C_k for different values of the shear width, Δz. The data points correspond to cases A1–A10, H1–H11 and I1–I12 in Tables A1 and A3.

the system, before settling back down towards zero, which is shown in Fig. 5. When the instability occurs large disturbances in B_y begin to appear and Fig. 5 shows that the rate of growth of B_y^2 is noticeably reduced as C_k decreased from the value set in our reference case, A1, which is 1.0×10^{-2}.

In this investigation we are principally interested in determining if an instability occurs so we focus our attention to the parts of the simulation long before boundary effects etc. are seen. For each of the cases we determine the maximum value of $\mathrm{d}(\ln B_y^2)/\mathrm{d}t$ and the time that it occurs after the initial transient phase. Fig. 6 shows the maximum value of $\mathrm{d}(\ln B_y^2)/\mathrm{d}t$ for cases A1–A10 where the only parameter that is varied is C_k. It shows that the maximum value of $\mathrm{d}(\ln B_y^2)/\mathrm{d}t$ tends to zero as we reduce C_k when $\Delta z = 1.0 \times 10^{-1}$ (the figure also shows other Δz cases that will be discussed later). A negative value for $\mathrm{d}(\ln B_y^2)/\mathrm{d}t$ indicates that B_y^2 is tending to zero, thus implying that there is no magnetic buoyancy instability. As the maximum value of $\mathrm{d}(\ln B_y^2)/\mathrm{d}t$ approaches zero it becomes difficult to accurately determine the maximum value due to numerical issues and so a spline interpolant is used to extrapolate from the values plotted to determine the value of C_k for which the instability no longer occurs, which is approximately 1.2×10^{-3}. Fig. 6 shows that by plotting B_y^2 for case A10, where $C_k = 1.25 \times 10^{-3}$, there is a small increase of B_y^2 with time. However, for case A11, where $C_k = 1.0 \times 10^{-3}$, there is a constant decrease. Thus we conclude that the instability is dependant on C_k being sufficiently large.

There is a criterion proposed to determine when the double-diffusive magnetic buoyancy instability might be present. Vasil & Brummell (2009) derived a new form of the criterion for magnetic buoyancy instability when a background state is constantly evolving. This is a more realistic model than that originally envisioned by Acheson who did not try to account for the back-reaction effect of the magnetic field on to a shear flow. The criterion proposed by Vasil & Brummell (2009) is expressed in a form where the magnetic field does not explicitly appear but where, instead, the shear flow that generates a layer of unstable magnetic field appears though the Richardson number and the width of the shear region itself. The analytic criterion derived by Vasil & Brummell (2009) for magnetic buoyancy in an isothermal process is

$$\frac{\Delta z}{4\gamma H_p}\left(1+\frac{\Delta z}{2H_\rho}\right) \gtrsim \frac{\zeta Ri}{(\gamma-1)\zeta+1}. \tag{10}$$

This expression shows that the threshold for instability will be affected not only by the ratio of magnetic to thermal diffusivities but also by the parameters associated with the shear forcing. While the double-diffusive magnetic buoyancy instabilities that we are investigating are not really isothermal they are closer to isothermal than adiabatic. We, therefore, will consider criteria (10) as a reference and now turn to examine how well this criterion is satisfied.

Fig. 7 shows, for the cases we are considering here, both the left-hand and right-hand sides of inequality (10) for different values of C_k and shows that the inequality is satisfied for the cases that lead to instability. The region where the inequality is satisfied covers a larger area for the higher values of C_k where we have already observed that the strength of the instability is at its greatest. While the criterion appears useful it should be noted that the inequality does, also, remain satisfied for small regions for some values of C_k that do not lead to instability (anything less than $C_k \approx 1.2 \times 10^{-3}$ is stable.). This is attributed to the fact that the stability criterion is analytically derived under assumptions for magnetic buoyancy instability in the isothermal limit so we would not expect complete agreement with the results. However, our findings show that this criterion is useful as a guide even when not fully in the isothermal regime.

Criterion (10) suggests that the regime where the instability will occur should also depend on a number of other parameters which include both the width of the shear flow and the magnitude of the shear flow. From observations, we only have an upper bound on the width of the tachocline and so it is important to understand how the width of the shear flow affects our findings. We adjust the width of the shear flow by varying Δz in equation (8).

Fig. 6, that was discussed earlier for the case when $\Delta z = 1.0 \times 10^{-1}$, also shows the maximum value of $\mathrm{d}(\ln B_y^2)/\mathrm{d}t$ plotted against the dimensionless thermal diffusivity, C_k, when the shear width is $\Delta z = 6.67 \times 10^{-2}$, which corresponds to cases H1–H12, and when $\Delta z = 5.0 \times 10^{-2}$, which corresponds to cases I1–I12. The spline interpolant curves through the data points are all similar in shape and Table 1 shows the critical values for each case. The critical value for C_k decreases as we reduce Δz; this implies that the greater the width of the region of shear is in the tachocline, the smaller the ratio of magnetic to thermal diffusivities must be to obtain magnetic buoyancy. Also, the maximum value of $\mathrm{d}(\ln B_y^2)/\mathrm{d}t$ for any given C_k is greater as we reduce Δz; this implies that the width of the shear region affects the strength of the instability. Given that at this present time we only have an upper bound on the width of the tachocline the results in this section suggest that if the tachocline is narrower then the ratio of magnetic to thermal diffusivities would need to be less extreme for this instability to occur. Further, a narrower tachocline would give rise to a more vigorous formation of strong structures.

Fig. 8(a) shows $\ln B_y^2$ plotted against time for different values of Δz (corresponding to cases A1, H1, I1, K1, L1 and M1) and shows that, when all other parameters are fixed, the instability onsets earlier

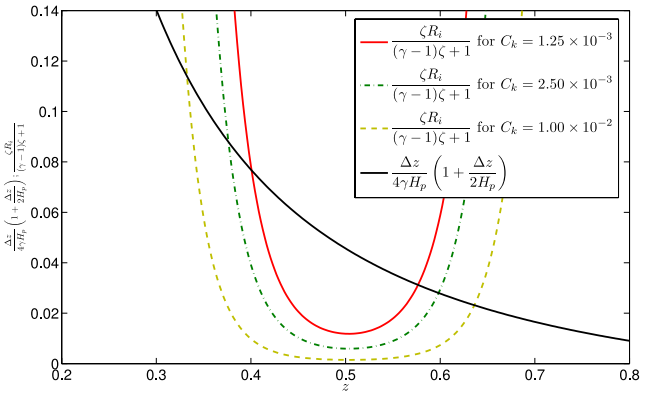

Figure 7. The solid black line that sweeps from the top left to the bottom right plots the left-hand side of inequality (10) versus depth (on the horizontal axis). The other three lines plot the right hand side for $C_k = 1.0 \times 10^{-2}$ (pale green dashed line), $C_k = 2.5 \times 10^{-3}$ (dark green dash–dotted line) and $C_k = 1.25 \times 10^{-3}$ (red solid line), all versus depth. The regions where these lines are below the black line are where the inequality is satisfied for instability.

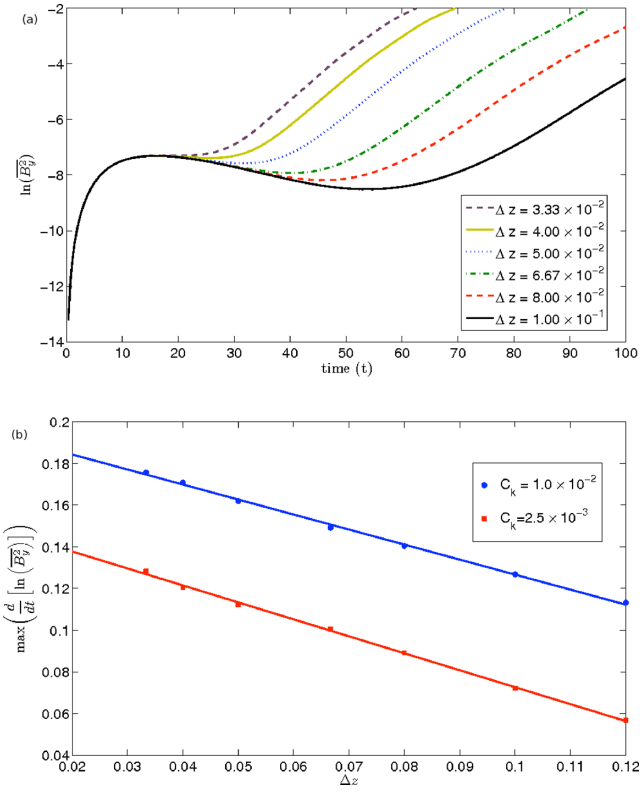

Figure 8. (a) $\ln B_y^2$ versus time for different values of the shear width, Δz. The data points correspond to cases A1, H1, I1, K1, L1, M1. (b) The maximum value of $\mathrm{d}(\ln B_y^2)/\mathrm{d}t$ versus the shear width, Δz. The data points for when $C_k = 1.0 \times 10^{-2}$ correspond to cases A1, H1, I1, K1, L1 and M1 and the data points for when $C_k = 2.5 \times 10^{-3}$ correspond to cases A6, H6, I6, K2, L2 and M2 in Tables A1 and A3.

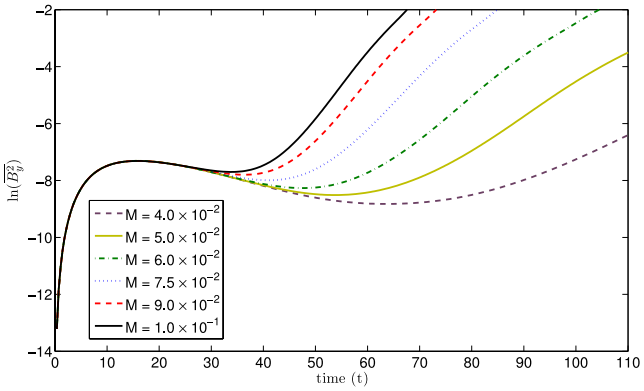

Figure 9. $\ln B_y^2$ versus time for different values of the shear magnitude, M. The data points correspond to cases A1, B1, C1, D1, E1 and F1 in Tables A1 and A2.

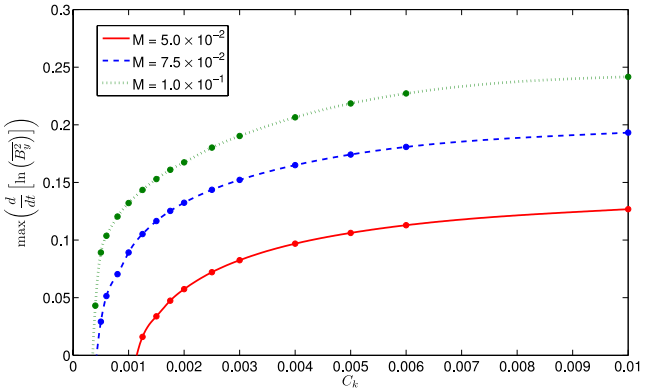

Figure 10. The maximum value of $\mathrm{d}(\ln B_y^2)/\mathrm{d}t$ versus the dimensionless thermal diffusivity, C_k, for different values of the shear magnitude, M. The data points correspond to cases A1–A10, B1–B14 and C1–C15 in Tables A1 and A2.

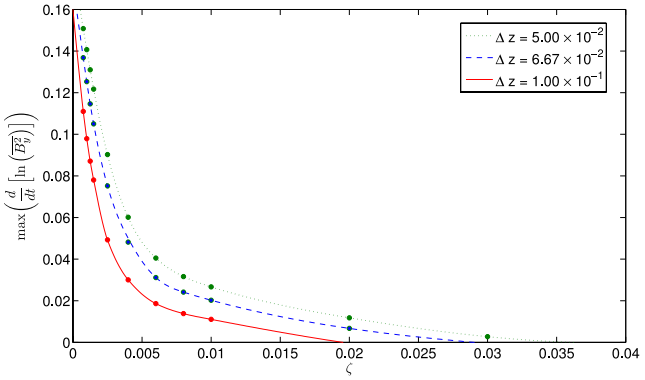

Figure 11. The maximum value of $\mathrm{d}(\ln B_y^2)/\mathrm{d}t$ versus ζ for different values of the shear width, Δz. The data points correspond to cases A1–A10, H1–H12 and I1–I12 from Tables A1 and A3.

as Δz is decreased. This is because the depth of the vertical region in which B_x is stretched out is determined by the shear width and, therefore, becomes narrower as Δz is reduced. The narrowing of this shear region causes the build up of B_x to happen faster, which is a result of the fact that B_x is dependent on the velocity gradient $\partial_z U_0(z)$ (Vasil & Brummell 2009). The faster build up and narrower shear region cause the gradients in B_x to reach the critical value for instability earlier and, therefore, the instability to occur sooner. We also note that the narrowing of the shear region also causes the instability to occur closer to the centre of the domain, $z = 0.5$.

The maximum value of $\mathrm{d}(\ln B_y^2)/\mathrm{d}t$ plotted against the shear width for $C_k = 2.5 \times 10^{-3}$ (cases A6, H6, I6, K2, L2, M2) and $C_k = 1.0 \times 10^{-2}$ (cases A1, H1, I1, K1, L1, M1) is shown in Fig. 8(b). This plot shows a linear relationship between the maximum growth rate of the instability and the width of the shear region. Therefore, this plot suggests that further decreasing the width of the shear flow region would give rise to a stronger instability but far greater resolution in z would be required to investigate smaller values of Δz than are presented here.

In addition to considering how varying the width of the shear flow affects the instability it is also interesting to also examine how the strength of the shear flow, governed by our parameter M, affects the results. This will allow us to comment on what may occur in other stars with a similar internal structure to the Sun but where the magnitude of the shear flow is different.

Cases A1, B1, C1, D1, E1 and F1 only differ in the shear magnitude value M. Fig. 9 shows that there is a non-linear relationship between M and the maximum value of $\mathrm{d}(\ln B_y^2)/\mathrm{d}t$ that is obtained for each of these cases. In Fig. 10, the maximum value of $\mathrm{d}(\ln B_y^2)/\mathrm{d}t$ is plotted against C_k for different values of M. In this figure two different M values, $M = 7.5 \times 10^{-2}$ and $M = 1.0 \times 10^{-1}$, are compared with the original case where $M = 5.0 \times 10^{-2}$ and shows that the critical value of C_K for the instability to occur becomes smaller as M is increased.

At the start of this section we commented on the fact that we wanted to consider the effect that varying the ratio of magnetic to thermal diffusivities has on the magnetic buoyancy instability and that there were two possible ways to change this ratio. First, we chose to maintain the magnetic diffusivity and vary the thermal diffusivity and so change the dynamics via the temperature equation and not the induction equation that evolves the magnetic field; the evolution of which is of greatest interest in this work. However, we could have chosen to vary the ratio via changing the magnetic diffusivity and so directly alter the induction equation. Given that one approach directly affects the evolution of the magnetic field and the other indirectly, through the temperature equation, these two approaches are not equivalent. Therefore, we will now briefly turn our attention to a discussion of the findings of how our results change, when Δz is varied, if we had selected the alternative approach where C_k is fixed and the non-dimensional parameter in our equations is changed through varying, η.

Fig. 11 shows how the maximum value of $\mathrm{d}(\ln B_y^2)/\mathrm{d}t$ varies as ζ is varied for different values of the shear width, Δz. The data in this figure corresponds to cases A1–A10 in Table 1 where $\Delta z = 1.0 \times 10^{-1}$, H1–H12 in Table A3 where $\Delta z = 6.67 \times 10^{-2}$ and I1–I12 in Table A3 where $\Delta z = 5.0 \times 10^{-2}$. Once again, we find that Fig. 11 shows that, for each value of Δz, there is a critical point that bounds the regime where the instability occurs. The critical point determines the greatest value of ζ for which the instability occurs. As we vary Δz we find critical values as follows: for $\Delta z = 5.0 \times 10^{-2}$ the critical value is approximately 3.599×10^{-2}, for $\Delta z = 6.67 \times 10^{-2}$ the critical value is approximately 2.89×10^{-2}, and for $\Delta z = 1.0 \times 10^{-1}$ the critical value is approximately 1.953×10^{-2}. Thus, for fixed C_k increasing the shear width increases the value below which instability occurs. We note though that for any given value of ζ for this fixed C_k investigation, decreasing the width of the shear region makes this instability more likely to occur. Thus, as was stated earlier for the variable C_k case, if

the tachocline is narrower than the ratio of magnetic to thermal instabilities would need to be less extreme for this instability to occur. Further, a narrower tachocline would give rise to a more vigorous formation of strong structures.

4 CONCLUSIONS

To obtain a full understanding of how the large-scale solar dynamo operates it is vital that we understand what conditions lead to buoyant structures being formed in the tachocline. There are still some unknowns when we are considering the tachocline region and further it is currently impossible to conduct full numerical simulations at the extreme values of some of the parameters. Therefore, it is important that we seek to explore how varying different quantities in the problem affect the formation of structures and to obtain scaling laws where possible.

In this paper we have presented the results from an investigation into the double-diffusive magnetic buoyancy instability. We chose to consider a quasi-two-dimensional model to enable a full exploration of how varying the key parameters associated with the problem affected the onset and initial phase of the instability. Our investigation primarily explored how varying the dimensionless thermal diffusivity, which varied the inverse Roberts number, affected the onset of the instability. The critical value for the thermal diffusivity translates into an upper bound on the ratio of magnetic to thermal diffusivity.

While in the tachocline we know that the ratio of magnetic to thermal diffusivities will be small, though exactly how small is not fully known, we still only have an upper bound at the present time on the thickness of the tachocline. Therefore, part of our research in this paper examined how the critical threshold value of the thermal diffusivity changed as we varied the width of the shear flow. We showed that varying the width of the shear flow by itself gives rise to a lower critical thermal diffusivity value for the onset of the instability. We have shown that the value of C_k for the instability to exist is dependent on the width of the shear region and the magnitude of the shear flow. Further, we have shown that the maximum value of the growth rate varies linearly with the width of the shear flow.

One of the principal motivations for undertaking this reduced study was to ascertain information that would inform later three-dimensional investigations to examine the evolution of structures formed by the double-diffusive instability. Our work has provided crucial information for such investigations as it has determined what part of the parameter space is unstable when $\sigma C_k = 2.5 \times 10^{-6}$ and $\zeta C_k = 5.0 \times 10^{-6}$. We have shown that for $M = 5.00 \times 10^{-2}$ the system is unstable for $\Delta z < 0.1$ provided $C_k > 1.25 \times 10^{-3}$. Further, we have shown that for fixed Δz, increasing M leads to a more unstable system. These results provide a firm foundation on which later three-dimensional investigations can be undertaken.

In the latter part of this paper, we discussed the effect of taking the alternative approach to this problem by varying the ratio of magnetic diffusivity to thermal diffusivity by altering the magnetic diffusivity. We showed that while the critical value of ζ, which translates into an effective value of the magnetic diffusivity, increases as you decrease the shear flow, for any given magnetic diffusivity (with all other parameters fixed) as you decrease the width of the shear flow it becomes increasingly likely that instability will occur.

This work has shown, as anticipated from earlier work, that there is a critical value for which the double-diffusive instability will occur. While the diffusive parameters that can be considered numerically are much larger than in the solar tachocline there will be a critical value of thermal diffusivity, at constant magnetic Prandtl number, for this instability to occur. Further, this work in varying the width of the shear flow region has shown that, if the solar tachocline is thinner than currently predicted, then double-diffusive magnetic buoyancy instability becomes more plausible as the ratio of magnetic to thermal diffusivities does not need to be so small for instability to occur. Once the width of the solar tachocline has been precisely determined, and the value of the transport coefficients obtained, we will be able to discuss fully if a double-diffusive magnetic buoyancy instability can exist in the tachocline.

Also, this work has provided a little insight into the magnetic buoyancy mechanism in other stars where the shear strength and width may be very different from the Sun. We have shown that as the strength of the shear is decreased, there appears to be a value below which the instability does not occur. This can be explained by the fact that sufficiently large gradients in the magnetic field are not being created to give rise to an instability and diffusive spreading of the generated magnetic field dominates. This would suggest that the presence of a tachocline in other stars would not be sufficient for magnetic buoyancy and, by current thinking for the solar cases, insufficient for a large-scale dynamo in other stars.

ACKNOWLEDGEMENTS

DMS would like to thank City University London for the award of a PhD studentship. We would like to thank the referee for very helpful suggestions and comments on the paper.

REFERENCES

Acheson D. J., 1979, Sol. Phys., 62, 23
Bushby P. J., Houghton S. M., 2005, MNRAS, 362, 313
Charbonneau P., 2010, Living Rev. Solar Phys. 7, 3
Cline K. S., Brummell N. H., Cattaneo F., 2003, ApJ, 599, 1449
Hughes D. W., Weiss N. 0., 1995, J. Fluid Mech., 301, 383
Jensen E., 1955, Ann. Astrophys., 18, 127
Newcomb W. A., 1961, Phys. Fluids, 4, 391
Parker E. N., 1955, ApJ, 121, 491
Parker E. N., 1966, ApJ, 145, 811
Parker E. N., 1993, ApJ, 408, 707
Schmitt J. H. M. M., Rosner R., 1983, ApJ, 265, 901
Silvers L. J., 2008, RSPTA, 366, 4453
Silvers L. J., Vasil G. M., Brummell N. H., Proctor M. R. E., 2009, ApJ, 702, L14
Thomas J. H., Nye A. H., 1975, Phys. Fluids, 18, 490
Tobias S. M., Hughes D. W., 2004, ApJ, 603, 785
Vasil G. M., Brummell N. H., 2008, ApJ, 686, 709
Vasil G. M., Brummell N. H., 2009, ApJ, 690, 783

APPENDIX A

Table A1. The parameter values for the cases discussed when varying C_k only.

	Prandtl number σ	Inverse Roberts number ζ	Dimensionless thermal diffusivity C_k	Maximum velocity for the shear M	Parameter controlling the width of the shear Δz	Richardson number Ri	Instability
A1	2.50×10^{-4}	5.00×10^{-4}	1.00×10^{-2}	5.00×10^{-2}	1.00×10^{-1}	2.96	Yes
A2	4.17×10^{-4}	8.33×10^{-4}	6.00×10^{-3}	5.00×10^{-2}	1.00×10^{-1}	2.96	Yes
A3	5.00×10^{-4}	1.00×10^{-3}	5.00×10^{-3}	5.00×10^{-2}	1.00×10^{-1}	2.96	Yes
A4	6.25×10^{-4}	1.25×10^{-3}	4.00×10^{-3}	5.00×10^{-2}	1.00×10^{-1}	2.96	Yes
A5	8.33×10^{-4}	1.67×10^{-3}	3.00×10^{-3}	5.00×10^{-2}	1.00×10^{-1}	2.96	Yes
A6	1.00×10^{-3}	2.00×10^{-3}	2.50×10^{-3}	5.00×10^{-2}	1.00×10^{-1}	2.96	Yes
A7	1.25×10^{-3}	2.50×10^{-3}	2.00×10^{-3}	5.00×10^{-2}	1.00×10^{-1}	2.96	Yes
A8	1.43×10^{-3}	2.86×10^{-3}	1.75×10^{-3}	5.00×10^{-2}	1.00×10^{-1}	2.96	Yes
A9	1.67×10^{-3}	3.33×10^{-3}	1.50×10^{-3}	5.00×10^{-2}	1.00×10^{-1}	2.96	Yes
A10	2.00×10^{-3}	4.00×10^{-3}	1.25×10^{-3}	5.00×10^{-2}	1.00×10^{-1}	2.96	Yes
A11	2.50×10^{-3}	5.00×10^{-3}	1.00×10^{-3}	5.00×10^{-2}	1.00×10^{-1}	2.96	No

Table A2. The parameter values for the additional cases needed when M is varied.

	Prandtl number σ	Inverse Roberts number ζ	Dimensionless thermal diffusivity C_k	Maximum velocity for the Shear M	Parameter Controlling the width of the shear Δz	Richardson Number Ri	Instability
B1	2.50×10^{-4}	5.00×10^{-4}	1.00×10^{-2}	7.50×10^{-2}	1.00×10^{-1}	1.32	Yes
B2	4.17×10^{-4}	8.33×10^{-4}	6.00×10^{-3}	7.50×10^{-2}	1.00×10^{-1}	1.32	Yes
B3	5.00×10^{-4}	1.00×10^{-3}	5.00×10^{-3}	7.50×10^{-2}	1.00×10^{-1}	1.32	Yes
B4	6.25×10^{-4}	1.25×10^{-3}	4.00×10^{-3}	7.50×10^{-2}	1.00×10^{-1}	1.32	Yes
B5	8.33×10^{-4}	1.67×10^{-3}	3.00×10^{-3}	7.50×10^{-2}	1.00×10^{-1}	1.32	Yes
B6	1.00×10^{-3}	2.00×10^{-3}	2.50×10^{-3}	7.50×10^{-2}	1.00×10^{-1}	1.32	Yes
B7	1.25×10^{-3}	2.50×10^{-3}	2.00×10^{-3}	7.50×10^{-2}	1.00×10^{-1}	1.32	Yes
B8	1.43×10^{-3}	2.86×10^{-3}	1.75×10^{-3}	7.50×10^{-2}	1.00×10^{-1}	1.32	Yes
B9	1.67×10^{-3}	3.33×10^{-3}	1.50×10^{-3}	7.50×10^{-2}	1.00×10^{-1}	1.32	Yes
B10	2.00×10^{-3}	4.00×10^{-3}	1.25×10^{-3}	7.50×10^{-2}	1.00×10^{-1}	1.32	Yes
B11	2.50×10^{-3}	5.00×10^{-3}	1.00×10^{-3}	7.50×10^{-2}	1.00×10^{-1}	1.32	Yes
B12	3.13×10^{-3}	6.25×10^{-3}	8.00×10^{-4}	7.50×10^{-2}	1.00×10^{-1}	1.32	Yes
B13	4.17×10^{-3}	8.33×10^{-3}	6.00×10^{-4}	7.50×10^{-2}	1.00×10^{-1}	1.32	Yes
B14	5.00×10^{-3}	1.00×10^{-2}	5.00×10^{-4}	7.50×10^{-2}	1.00×10^{-1}	1.32	Yes
B15	6.25×10^{-3}	1.25×10^{-2}	4.00×10^{-4}	7.50×10^{-2}	1.00×10^{-1}	1.32	No
C1	2.50×10^{-4}	5.00×10^{-4}	1.00×10^{-2}	1.00×10^{-1}	1.00×10^{-1}	0.74	Yes
C2	4.17×10^{-4}	8.33×10^{-4}	6.00×10^{-3}	1.00×10^{-1}	1.00×10^{-1}	0.74	Yes
C3	5.00×10^{-4}	1.00×10^{-3}	5.00×10^{-3}	1.00×10^{-1}	1.00×10^{-1}	0.74	Yes
C4	6.25×10^{-4}	1.25×10^{-3}	4.00×10^{-3}	1.00×10^{-1}	1.00×10^{-1}	0.74	Yes
C5	8.33×10^{-4}	1.67×10^{-3}	3.00×10^{-3}	1.00×10^{-1}	1.00×10^{-1}	0.74	Yes
C6	1.00×10^{-3}	2.00×10^{-3}	2.50×10^{-3}	1.00×10^{-1}	1.00×10^{-1}	0.74	Yes
C7	1.25×10^{-3}	2.50×10^{-3}	2.00×10^{-3}	1.00×10^{-1}	1.00×10^{-1}	0.74	Yes
C8	1.43×10^{-3}	2.86×10^{-3}	1.75×10^{-3}	1.00×10^{-1}	1.00×10^{-1}	0.74	Yes
C9	1.67×10^{-3}	3.33×10^{-3}	1.50×10^{-3}	1.00×10^{-1}	1.00×10^{-1}	0.74	Yes
C10	2.00×10^{-3}	4.00×10^{-3}	1.25×10^{-3}	1.00×10^{-1}	1.00×10^{-1}	0.74	Yes
C11	2.50×10^{-3}	5.00×10^{-3}	1.00×10^{-3}	1.00×10^{-1}	1.00×10^{-1}	0.74	Yes
C12	3.13×10^{-3}	6.25×10^{-3}	8.00×10^{-4}	1.00×10^{-1}	1.00×10^{-1}	0.74	Yes
C13	4.17×10^{-3}	8.33×10^{-3}	6.00×10^{-4}	1.00×10^{-1}	1.00×10^{-1}	0.74	Yes
C14	5.00×10^{-3}	1.00×10^{-2}	5.00×10^{-4}	1.00×10^{-1}	1.00×10^{-1}	0.74	Yes
C15	6.25×10^{-3}	1.25×10^{-2}	4.00×10^{-4}	1.00×10^{-1}	1.00×10^{-1}	0.74	Yes
C16	8.33×10^{-3}	1.67×10^{-2}	3.00×10^{-4}	1.00×10^{-1}	1.00×10^{-1}	0.74	No
D1	2.50×10^{-4}	5.00×10^{-4}	1.00×10^{-2}	9.00×10^{-2}	1.00×10^{-1}	0.92	Yes
E1	2.50×10^{-4}	5.00×10^{-4}	1.00×10^{-2}	6.00×10^{-2}	1.00×10^{-1}	2.06	Yes
F1	2.50×10^{-4}	5.00×10^{-4}	1.00×10^{-2}	4.00×10^{-2}	1.00×10^{-1}	4.63	Yes
G1	2.50×10^{-4}	5.00×10^{-4}	1.00×10^{-2}	3.00×10^{-2}	1.00×10^{-1}	8.24	Yes

Table A3. The parameter values for the additional cases required when Δz is varied.

	Prandtl number σ	Inverse Roberts number ζ	Dimensionless thermal diffusivity C_k	Maximum velocity for the shear M	Parameter controlling the width of the shear Δz	Richardson number Ri	Instability
H1	2.50×10^{-4}	5.00×10^{-4}	1.00×10^{-2}	5.00×10^{-2}	6.67×10^{-2}	1.32	Yes
H2	4.17×10^{-4}	8.33×10^{-4}	6.00×10^{-3}	5.00×10^{-2}	6.67×10^{-2}	1.32	Yes
H3	5.00×10^{-4}	1.00×10^{-3}	5.00×10^{-3}	5.00×10^{-2}	6.67×10^{-2}	1.32	Yes
H4	6.25×10^{-4}	1.25×10^{-3}	4.00×10^{-3}	5.00×10^{-2}	6.67×10^{-2}	1.32	Yes
H5	8.33×10^{-4}	1.67×10^{-3}	3.00×10^{-3}	5.00×10^{-2}	6.67×10^{-2}	1.32	Yes
H6	1.00×10^{-3}	2.00×10^{-3}	2.50×10^{-3}	5.00×10^{-2}	6.67×10^{-2}	1.32	Yes
H7	1.25×10^{-3}	2.50×10^{-3}	2.00×10^{-3}	5.00×10^{-2}	6.67×10^{-2}	1.32	Yes
H8	1.67×10^{-3}	3.33×10^{-3}	1.50×10^{-3}	5.00×10^{-2}	6.67×10^{-2}	1.32	Yes
H9	2.00×10^{-3}	4.00×10^{-3}	1.25×10^{-3}	5.00×10^{-2}	6.67×10^{-2}	1.32	Yes
H10	2.50×10^{-3}	5.00×10^{-3}	1.00×10^{-3}	5.00×10^{-2}	6.67×10^{-2}	1.32	Yes
H11	2.78×10^{-3}	5.56×10^{-3}	9.00×10^{-4}	5.00×10^{-2}	6.67×10^{-2}	1.32	Yes
H12	3.13×10^{-3}	6.25×10^{-3}	8.00×10^{-4}	5.00×10^{-2}	6.67×10^{-2}	1.32	No
I1	2.50×10^{-4}	5.00×10^{-4}	1.00×10^{-2}	5.00×10^{-2}	5.00×10^{-2}	0.74	Yes
I2	4.17×10^{-4}	8.33×10^{-4}	6.00×10^{-3}	5.00×10^{-2}	5.00×10^{-2}	0.74	Yes
I3	5.00×10^{-4}	1.00×10^{-3}	5.00×10^{-3}	5.00×10^{-2}	5.00×10^{-2}	0.74	Yes
I4	6.25×10^{-4}	1.25×10^{-3}	4.00×10^{-3}	5.00×10^{-2}	5.00×10^{-2}	0.74	Yes
I5	8.33×10^{-4}	1.67×10^{-3}	3.00×10^{-3}	5.00×10^{-2}	5.00×10^{-2}	0.74	Yes
I6	1.00×10^{-3}	2.00×10^{-3}	2.50×10^{-3}	5.00×10^{-2}	5.00×10^{-2}	0.74	Yes
I7	1.25×10^{-3}	2.50×10^{-3}	2.00×10^{-3}	5.00×10^{-2}	5.00×10^{-2}	0.74	Yes
I8	1.67×10^{-3}	3.33×10^{-3}	1.50×10^{-3}	5.00×10^{-2}	5.00×10^{-2}	0.74	Yes
I9	2.00×10^{-3}	4.00×10^{-3}	1.25×10^{-3}	5.00×10^{-2}	5.00×10^{-2}	0.74	Yes
I10	2.50×10^{-3}	5.00×10^{-3}	1.00×10^{-3}	5.00×10^{-2}	5.00×10^{-2}	0.74	Yes
I11	2.78×10^{-3}	5.56×10^{-3}	9.00×10^{-4}	5.00×10^{-2}	5.00×10^{-2}	0.74	Yes
I12	3.13×10^{-3}	6.25×10^{-3}	8.00×10^{-4}	5.00×10^{-2}	5.00×10^{-2}	0.74	Yes
I13	3.57×10^{-3}	7.14×10^{-3}	7.00×10^{-4}	5.00×10^{-2}	5.00×10^{-2}	0.74	No
J1	2.50×10^{-4}	5.00×10^{-4}	1.00×10^{-2}	5.00×10^{-2}	1.20×10^{-1}	4.27	Yes
J2	1.00×10^{-3}	2.00×10^{-3}	2.50×10^{-3}	5.00×10^{-2}	1.20×10^{-1}	4.27	Yes
K1	2.50×10^{-4}	5.00×10^{-4}	1.00×10^{-2}	5.00×10^{-2}	8.00×10^{-2}	1.90	Yes
K2	1.00×10^{-3}	2.00×10^{-3}	2.50×10^{-3}	5.00×10^{-2}	8.00×10^{-2}	1.90	Yes
L1	2.50×10^{-4}	5.00×10^{-4}	1.00×10^{-2}	5.00×10^{-2}	4.00×10^{-2}	0.48	Yes
L2	1.00×10^{-3}	2.00×10^{-3}	2.50×10^{-3}	5.00×10^{-2}	4.00×10^{-2}	0.48	Yes
M1	2.50×10^{-4}	5.00×10^{-4}	1.00×10^{-2}	5.00×10^{-2}	3.33×10^{-2}	0.33	Yes
M2	1.00×10^{-3}	2.00×10^{-3}	2.50×10^{-3}	5.00×10^{-2}	3.33×10^{-2}	0.33	Yes

This paper has been typeset from a TEX/LATEX file prepared by the author.